

## Dephasingless plasma wakefield photon acceleration

R. Sandberg \* and A. G. R. Thomas †

*G erard Mourou Center for Ultrafast Optical Sciences, University of Michigan, Ann Arbor, Michigan 48109, USA*



(Received 16 October 2023; accepted 22 January 2024; published 16 February 2024)

Sandberg and Thomas [Phys. Rev. Lett. **130**, 085001 (2023)] proposed a scheme to generate ultrashort, high-energy pulses of XUV photons through dephasingless photon acceleration in a beam-driven plasma wakefield. An ultrashort laser pulse is placed in the plasma wake behind a relativistic electron bunch such that it experiences a comoving negative density gradient and therefore shifts up in frequency. Using a tapered density profile provides phase-matching between driver and witness pulses. In this paper, we give the details of the wakefield solutions and phase-matching conditions used to generate the phase-matching density profile. The short, high-density, and weak driver limits are considered. We show, explicitly, the numerical algorithm used to calculate the density profiles.

DOI: [10.1103/PhysRevE.109.025210](https://doi.org/10.1103/PhysRevE.109.025210)

### I. INTRODUCTION

The many applications of bright, coherent XUV light have motivated substantial interest in source development, such as the construction of XUV wavelength free electron lasers such as FLASH [1] as well as nonlinear frequency mixing [2], high harmonic generation [3], relativistic flying mirrors [4–6], and XUV lasing [7], to name a few. Another method for generating short wavelengths is photon acceleration [8,9].

From the linear, unmagnetized plasma dispersion relation  $\omega^2 = k^2c^2 + \omega_p^2$ , where  $\omega_p^2 = e^2n/m_e\epsilon_0$  for a plasma of number density  $n$ , it can be seen that if we identify a localized electromagnetic energy wave packet with central frequency  $\omega$  as a quasiphoton and consider its quasiphoton energy and momentum  $E = \hbar\omega$  and  $\vec{p} = \hbar\vec{k}$ , when propagating in the background plasma it will gain an effective mass  $\hbar\omega_p/c^2$ . The wave-packet group velocity is  $\vec{v}_g = \vec{k}/\omega$  and hence if its frequency is up-shifted, the dispersion relation implies that the quasiphoton will travel at a higher velocity, i.e., it is accelerated. In the presence of copropagating density gradients, the quasiphotons experience local frequency shifts due to spatiotemporal variations in the phase velocity [10] and are therefore accelerated. The resulting quasiphoton phase-space trajectories in plasma wakefields are similar to those of leptons [11].

Photon acceleration can arise as a result of plasma wakefields [8], ionization fronts [12,13], and even using metamaterials [14]. Photon acceleration was measured in ionization front [15] and laser wakefield acceleration experiments [16,17]. Recent results include cascaded sequences of localized ionizations [18], resulting in large frequency shifts and the use of plasma wakes to downshift radiation to very long wavelengths [19]. Limits to photon acceleration in plasma

wakefields in the linear [20] and nonlinear regimes [21,22] were previously studied, identifying dephasing of the photon beam with respect to the accelerating refractive index gradient as placing a ceiling on the frequency shift. Dephasing occurs when the difference between the phase velocity of the wake and the high-frequency photon pulse results in it slipping out of the accelerating refractive index gradient. A recent scheme for overcoming this restriction using an ionization front is dephasingless frequency shift using a flying focus, a combination of a chirped laser pulse and an achromatic lens for spatiotemporal shaping of a laser pulse [23]. The flying focus was also used to mitigate the analogous process of electron beam dephasing in a plasma wakefield [24], in addition to related spatiotemporally structured focusing schemes [25,26].

Another method for mitigating dephasing in the context of electron acceleration is the use of tapered plasma density ramps [27–30]. By having a nonuniform density, the plasma wavelength varies along the propagation length, which allows for locking the accelerating phase with the particle beam. Tapered density ramps were previously suggested as a way of increasing the frequency shifts in photon acceleration [8,20]. In our recent paper [31], we showed that by using a relativistic-charged-particle-beam driven photon accelerator with a tapered density ramp, dephasing could be mitigated and large frequency shifts were possible, limited only by the available driver energy. With a beam driver, we found that the appropriate density profile is a down ramp rather than the up ramp considered in previous studies of the laser driven case. We refer to this as the dephasingless plasma wakefield photon acceleration (dePWPA). In one-dimensional *ab initio* relativistic electromagnetic particle-in-cell simulations we demonstrated a more than 50 times frequency shift.

In this paper, we expand on the details of the analytic model used for the results of Ref. [31], including the derivation of the beam-driven wakefield solution and the phase matching condition and validate approximations in the short driver limit. We also explicitly give the algorithm used to solve the equations to calculate the tapered density profile needed to

\*Present address: Lawrence Berkeley National Laboratory, Berkeley, California 94720, USA; [rsandberg@lbl.gov](mailto:rsandberg@lbl.gov)

†[agrt@umich.edu](mailto:agrt@umich.edu)

mitigate dephasing. In Sec. II, we review the frequency shift and phase-matching condition required for dePWPA given in our previous paper [31] for completeness. In Sec. III, we develop the solution for the wakefield given behind an arbitrary density and length beam driver pulse; the one-dimensional wake solutions for a wakefield driven by a top-hat profile beam were developed by Rosenzweig [32] for the weak driver beam case,  $n_d/n < \frac{1}{2}$ , where  $n_d$  is the drive-beam density. We extend this model to solutions for arbitrary drive-beam density  $n_d/n \geq \frac{1}{2}$ . In Sec. IV, we show the method for solving the dephasing condition, including the computational algorithm (the actual Python code used to calculate the density maps used in Ref. [31] is also included as Supplemental Material [33]). In Sec. V, we study the approximations to the solutions in the short, high-density (SHD), and weak driver limits. In particular, we show that as the plasma density drops for the dephasingless scheme, the driver approaches the SHD limit and so the SHD limit is valid initially for a large fraction of initial beam parameters and asymptotically for all beam parameters. Finally, we conclude in Sec. VI.

## II. DEPHASINGLESS PHOTON ACCELERATION

### A. Frequency shifts in the presence of a density gradient

A laser pulse that experiences a comoving plasma density gradient will be upshifted in frequency. From eikonal solutions to the wave equation, well-known ray-tracing solutions can be used for the temporal variation in the light [9,34] to relate it to the density gradients generated in a wakefield. For a given dispersion relation  $D$ , the frequency  $\omega$  and wave number  $k_z$  of an optical mode propagating in the  $z$  direction satisfy the following relations:

$$\begin{aligned} dz/d\tau &= \partial D/\partial k_z, & dk_z/d\tau &= -\partial D/\partial z, \\ dt/d\tau &= \partial D/\partial \omega, & d\omega/d\tau &= \partial D/\partial t. \end{aligned} \quad (1)$$

The optical mode will vary with distance propagated as

$$\frac{d\omega}{dz} = \frac{d\omega/d\tau}{dz/d\tau} = \frac{\partial D/\partial t}{\partial D/\partial k_z}. \quad (2)$$

We assume that the laser pulse is propagating in a wakefield generated by a relativistic driver (either a relativistic particle beam or second laser pulse) propagating at velocity  $v_d(z)$  and therefore change coordinates from  $(x, y, z, t)$  to  $(x, y, z, \zeta = t - \int_0^z dz'/v_d(z'))$  [28]. The change in the frequency can, therefore, be expressed as

$$\frac{d\omega}{dz} = \frac{\partial D/\partial \zeta}{\partial D/\partial k_z}. \quad (3)$$

For example, for linear plasma dispersion,  $D = \omega^2 - \omega_p^2/\gamma - k^2 c^2$ , and assuming that ions are immobile and the variations in the plasma density with respect to  $\zeta$  are much larger than the variations in  $\omega$  and  $k$ :

$$\frac{d\omega}{dz} \simeq \frac{1}{2k_z c^2} \frac{\partial(\omega_p^2/\gamma)}{\partial \zeta}. \quad (4)$$

Note that the  $\gamma$  factor in the linear dispersion relation is to allow for relativistically streaming electrons rather than, e.g., oscillations in the laser field, and therefore this dispersion relation is considered exact for a weak laser pulse.

### B. Matching condition to mitigate dephasing

For positive frequency shift, the laser pulse must be at a phase in the wake where the density is gradient and is positive with respect to the coordinate  $\zeta$ . However, the laser centroid moves at the group velocity of the laser pulse and so, as the laser pulse shifts in frequency, its group velocity increases and the pulse will change position in the wake. To mitigate dephasing of the photon pulse, we use a tapered density profile (similar to that proposed for mitigating dephasing in electron acceleration [28,30,35,36]) to continuously increase the plasma wavelength and keep the laser pulse experiencing a positive plasma density gradient.

Here, we derive the phase-matching condition for a one-dimensional (1D) nonlinear plasma wake, which we find is also accurate to describe the three-dimensional case for a broad driver ( $k_p \sigma_r \gg 1$ ), where  $k_p = \omega_p/c$  and  $\sigma_r$  is the root-mean-square beam radius. Under the assumption that  $d \log(n)/dz \ll k_p(z)$  for all  $z$ , i.e., the plasma density gradients are long compared to the wake period scale, to lowest order the wake may be assumed to follow the uniform plasma solution with local density  $n(z)$ . Hence, we write the perturbed density of the wake  $n_w(\zeta; z)$  as a function of  $\zeta$  parameterized by  $z$ , i.e., by the local density  $n(z)$ .

For convenience, we choose the point where the density perturbation in the wake  $\delta n(\zeta; z) \equiv n_w(\zeta; z) - n(z) = 0$  within the region of positive density gradient, hereby labeled as  $\zeta_\delta$ , as the location of the reference density gradient we are trying to track. This is not the maximum density gradient except in the linear regime, but the maximum is, in general, only slightly behind  $\zeta_\delta$ , and using  $\zeta_\delta$  greatly simplifies the analysis. It can be shown that the maximum refractive index gradient occurs where the electric field of the wake is zero, which is close to where the density perturbation goes to zero. It can also be shown that the refractive index gradient is equal to the density gradient at the point where  $\delta n = 0$  for a 1D wake.

To keep the pulse experiencing the greatest possible frequency shift, we require  $\zeta_{\text{centroid}} = \zeta_\delta$  for all times, where  $\zeta_{\text{centroid}}$  denotes the center of the witness laser pulse. Expressed in differential form, we have

$$\frac{d\zeta_{\text{centroid}}}{dz} = \frac{d\zeta_\delta}{dz}, \quad (5)$$

which may be written as

$$\frac{1}{v_{\text{centroid}}} - \frac{1}{v_d} = \frac{d\zeta_d}{dn} \frac{dn}{dz}. \quad (6)$$

For an ultrarelativistic particle beam driver, we make the approximation  $v_d \rightarrow c$ . Assuming that the laser pulse moves at the linear group velocity and the plasma is underdense,  $\omega_p^2/\omega^2 \ll 1$ , we obtain an equation relating the  $z$  profile of the plasma number density to the variation in the wake position of the zero density perturbation  $\zeta_\delta$  with plasma density:

$$\frac{dn}{dz} \simeq \frac{1}{2c} \frac{\omega_p^2}{\omega^2} \left[ \frac{d\zeta_\delta}{dn} \right]^{-1}. \quad (7)$$

Note that  $\gamma(\zeta_\delta) = 1$ , where the density perturbation is zero.

The phase-matching condition in Eq. (7) and the frequency-shift relation in Eq. (4) together are a coupled pair

of differential equations for the plasma density profile that will give phase-matched photon acceleration as well as the predicted frequency shift given the phase matched density profile. To close them, it remains to determine the dependence of the quantities  $\frac{\partial(\omega_p^2/\gamma)}{\partial\zeta}|_{\zeta_\delta}$  and  $\frac{d\zeta_\delta}{dn}$  on  $n$  and  $\omega$ .

### III. DESCRIPTION OF THE WAKE BEHIND THE DRIVER

In this section, the position  $\zeta_\delta$  in the wake where  $\delta n = 0$  and there is a positive density gradient is obtained, along with the density gradient at that position. We derive these quantities using a 1D model for the wakefield, which we find is accurate to describe the three-dimensional case in the broad driver ( $k_p\sigma_r \gg 1$ ) approximation, where  $k_p = \omega_p/c$  and  $\sigma_r$  is the root-mean-square beam radius. The wake behind the driver is modeled with the 1D Akhiezer-Polovin (AP) [37] relativistic wave. This is an undriven plasma wave with a given amplitude  $\gamma_m$  and phase velocity  $\beta_w = v_p/c$ ; in this paper, the wave phase velocity is assumed to be ultrarelativistic,  $\beta_w \rightarrow 1$ .

For clarity, we express the equations in normalized units, with all plasma densities  $n \rightarrow n/n_0$  where  $n_0$  is a reference plasma density. Also  $\omega_p \rightarrow \omega_p/\omega_{p0}$ ,  $\omega \rightarrow \omega/\omega_{p0}$ ,  $p \rightarrow p/m_e c$ , etc., where  $\omega_{p0}^2 = e^2 n_0/m_e \epsilon_0$ ,  $E \rightarrow eE/mc\omega_{p0}$ , etc.

The Lagrangian form of the plasma equations describing the AP wave is used here to develop a solution parameterized in terms of a periodic coordinate  $\varphi$  as derived by Infeld and Rowlands in Ref. [38] (particularly, the expression of the Infeld-Rowland-Akhiezer-Polovin wave derived in Verma *et al.* [39,40].) With the parametrization of the wake behind the driver, the position of zero density perturbation,  $\zeta_\delta$ , and the plasma density gradient there,  $\frac{\partial(\omega_p^2/\gamma)}{\partial\zeta}|_{\zeta_\delta}$ , are found as functions of the wake parameters  $\varphi_{st}$  and amplitude  $\gamma_m$  defining the wake behind the driver. Then, the dependence of the starting phase  $\varphi_{st}$  on the wake within the driver is found, particularly on the fluid Lorentz factor  $\gamma_d$ , momentum  $p_d$ , and electric field  $E_{zd}$  at the end of the driver. The dependence of the wake amplitude  $\gamma_m$  on fluid quantities in the wake will be determined in the subsequent section.

Under the assumption that  $d \log(n)/dz \ll k_p(z)$  for all  $z$ , i.e., the plasma density gradients are long compared to the wake period scale, to lowest order the wake may be assumed to follow the uniform plasma solution with local density  $n(z)$ . Hence, the density in the wake  $n_w(\zeta; z)$  is a function of  $\zeta$  and is parameterized by  $z$ , i.e., by the local density  $n(z)$ .

Because  $n(z)$  changes slowly compared to  $n_w(\zeta, z)$ , we find the dependence of  $n_w(\zeta, z)$  at fixed  $z$ . In this section, we will stop explicitly writing the  $z$  dependence, i.e.,  $n_w(\zeta; z) = n_w(\zeta)$  and  $n = n(z)$ .

The AP solution to the cold relativistic fluid equations has the form [37,39]

$$\omega_p \zeta = \frac{2}{\kappa'} E(\varphi, \kappa^2) - \kappa' F(\varphi, \kappa^2) - \frac{1}{\beta} \frac{2\kappa}{\kappa'} \sin \varphi, \quad (8a)$$

$$\gamma(\varphi) = \gamma_m - (\gamma_m - 1) \sin^2(\varphi), \quad (8b)$$

$$p(\varphi, \gamma) = \cos \varphi \sqrt{\gamma_m - 1} \sqrt{1 + \gamma}, \quad (8c)$$

$$qE_z(\varphi) = \sin \varphi \sqrt{2(\gamma_m - 1)}, \quad (8d)$$

$$\beta(\varphi, \gamma) = p(\varphi, \gamma)/\gamma, \quad (8e)$$

$$n_w(\beta) = n(1 - \beta)^{-1}, \quad (8f)$$

$$\kappa^2 = \frac{\gamma_m - 1}{\gamma_m + 1}, \quad (8g)$$

$$\kappa'^2 = \frac{2}{\gamma_m + 1}, \quad (8h)$$

where  $F(\varphi, \kappa^2)$  and  $E(\varphi, \kappa^2)$  are elliptic integrals of the first and second kind, respectively, and parameters  $\varphi = 2n\pi$  correspond to maxima in the plasma density and  $\varphi = j + \pi/2$ , where  $j \in \mathbb{Z}$ , correspond to points of zero perturbation,  $n_w = n$ . Furthermore, we will demonstrate soon that  $\varphi = (2j + 3/2)\pi$  corresponds to points of zero perturbation and increasing plasma density,  $\partial n_w/\partial\zeta > 0$ . These equations completely describe the wake behind the drive electron beam given the mapping from drive beam to amplitude  $\gamma_m$  and starting parameter  $\varphi_{st}$ .

With the wake behind the driver completely described in terms of amplitude  $\gamma_m$  and parameter  $\varphi_{st}$ , the quantities  $\zeta_\delta$  and  $\frac{\partial(\omega_p^2/\gamma)}{\partial\zeta}|_{\zeta_\delta}$  may be derived. The position  $\zeta_\delta$ , measured from the leading edge of the drive beam, can be expressed as

$$\zeta_\delta = \zeta(3\pi/2) - \zeta(\varphi_{st}) + L_d/c, \quad (9)$$

where  $\zeta(\varphi)$  is the position in the undriven wake as a function of  $\varphi$ ,  $L_d$  is the length of the drive beam, and  $\varphi_{st}$  is determined so the wake is continuous across the transition from drive beam to undriven wake. To enforce continuity of the wake, we will require that electric field and momentum are continuous at the transition from within the drive beam to behind the drive beam. Let  $\gamma_d$  denote the plasma Lorentz factor at the end of the drive beam,  $p_d$  be the plasma momentum at the end of the drive beam, and  $E_{zd}$  the electric field at the end of the driver. The equations for  $p$  and  $E_z$  behind the driver can be arranged to determine  $\varphi$  in terms of fluid quantities:

$$\cos \varphi = \frac{p}{\sqrt{\gamma_m - 1} \sqrt{1 + \gamma}}, \quad (10a)$$

$$\sin \varphi = \frac{qE_z}{\sqrt{2(\gamma_m - 1)}}. \quad (10b)$$

These equations combine to determine  $\tan \varphi_{st}$  as a function of the fluid quantities:

$$\tan \varphi_{st} = \frac{qE_{zd}}{p_d} \sqrt{\frac{1 + \gamma_d}{2}}. \quad (11)$$

Now  $\varphi_{st}$  is determined by the fluid quantities within the drive beam. The dependence of these on the drive-beam parameters will be derived in the next section.

Next, the dependence of  $\frac{\partial(\omega_p^2/\gamma)}{\partial\zeta}|_{\zeta_\delta}$  on the unperturbed plasma density  $n$  and the wake amplitude  $\gamma_m$  is determined. Because  $\omega_p^2$  is proportional to  $n_w$  with constant of proportionality  $e^2/m_e \epsilon_0$ , it suffices to calculate  $\partial(n_w/\gamma)/\partial\zeta|_{\zeta_\delta}$ . Because evolution in  $z$  is considered to be much slower than evolution in  $\zeta$ , in this section  $n$ ,  $\omega_p$ ,  $\gamma_m(z)$ ,  $\beta$ ,  $\kappa$ , and  $\kappa'$  are treated as constants. Hence all quantities ultimately depend only on  $\zeta$  and we will derive  $d(n_w/\gamma)/d\zeta|_{\zeta_\delta}$ . When  $\delta n = 0$ , then  $n_w = n$  so  $\beta = p = 0$ ,  $\gamma = 1$ , and  $\varphi = \varphi_j \equiv (j + 1/2)\pi$  with  $j \in \mathbb{Z}$ .

First, we note that  $\frac{d(n_w/\gamma)}{d\zeta}|_{\zeta_\delta} = \frac{dn_w}{d\zeta}|_{\zeta_\delta}$ , by observing that  $\frac{d\gamma}{d\zeta}|_{\zeta_\delta} = 0$ . Then, because  $\gamma_m(\varphi_j) = 1$ , we have

$$\frac{d(n_w/\gamma)}{d\zeta}\Big|_{\zeta_\delta} = \frac{dn_w}{d\zeta}\Big|_{\zeta_\delta} = \frac{dn_w}{d\beta}\Big|_{\beta=0} \frac{d\beta}{d\varphi}\Big|_{\varphi=\varphi_j} \frac{d\varphi}{d\zeta}\Big|_{\zeta_\delta}. \quad (12)$$

Performing the substitutions yields the plasma gradient where  $\delta n = 0$ :

$$\frac{dn_w}{d\zeta}\Big|_{\zeta_\delta} = n(z)(-\sin(\varphi_j))\sqrt{2(\gamma_m - 1)}\omega_p(z). \quad (13)$$

The positive plasma gradient required for positive frequency shift then means we want odd values of  $j$ , i.e., for  $l \in \mathbb{Z}$ , values  $\varphi_{2l+1} = (2l + \frac{3}{2})\pi$ . We can now write

$$\frac{d(\omega_p^2/\gamma)}{d\zeta}\Big|_{\zeta_\delta} = \omega_p(z)n(z)\sqrt{2(\gamma_m - 1)}. \quad (14)$$

In this section, we have modeled the wake behind the driver as a traveling relativistic plasma wave. We presented a periodic parametrization of this wave and derived from this representation quantities  $\zeta_\delta$  and  $\frac{\partial\omega_p^2/\gamma}{\partial\zeta}|_{\zeta_\delta}$  necessary for understanding frequency shift and phase matching. It remains to determine the dependence of the amplitude  $\gamma_m$  on the drive-beam density  $n_d$  and length  $L_d$ , as well as the dependence of fluid quantities at the end of the drive beam on the drive-beam parameters. The quantities we want at the drive-beam end are the electric field  $E_{zd}$ , fluid momentum  $p_d$ , and fluid gamma factor  $\gamma_d$ .

### A. Solution within drive beam

In the previous section, we determined the dependence of  $\zeta_\delta$  and  $\frac{\partial(\omega_p^2/\gamma)}{\partial\zeta}|_{\zeta_\delta}$  on the values of the fluid electric field, momentum, and Lorentz factor at the end of the drive beam,  $E_{zd}$ ,  $p_d$ , and  $\gamma_d$ . To determine these expressions, we determine the fluid equations within the drive beam as a function of  $\zeta$  and evaluate the solution at the end of the drive beam,  $\zeta = L_d$ . We follow the solution technique in Ref. [32], parametrizing the fluid quantities by a quantity  $x$ :

$$\gamma = \frac{1+x^2}{2x}, \quad (15a)$$

$$p = \frac{1-x^2}{2x}, \quad (15b)$$

$$E_z = \frac{\partial x}{\partial \zeta} = \text{sgn}(E_z) \sqrt{2\left(1 - \frac{n_d}{n}\right) - \frac{1}{x} + \left(\frac{2n_d}{n} - 1\right)x}, \quad (15c)$$

$$\phi = 1 - x. \quad (15d)$$

The parameter  $x$  satisfies the equation

$$\frac{\partial^2 x}{\partial \zeta^2} = \frac{1}{2} \left( \frac{1}{x^2} - 1 + \frac{2n_d}{n} \right). \quad (16)$$

The form of the solution is different for each of the three cases  $0 < n_d < n/2$ ,  $n_d = n/2$ , and  $n_d > n/2$ ; see Appendix A for the full derivation. We write here the expressions for the parameter  $x$  at  $\zeta = L_d$ , denoted  $x_d$ , in the three cases.

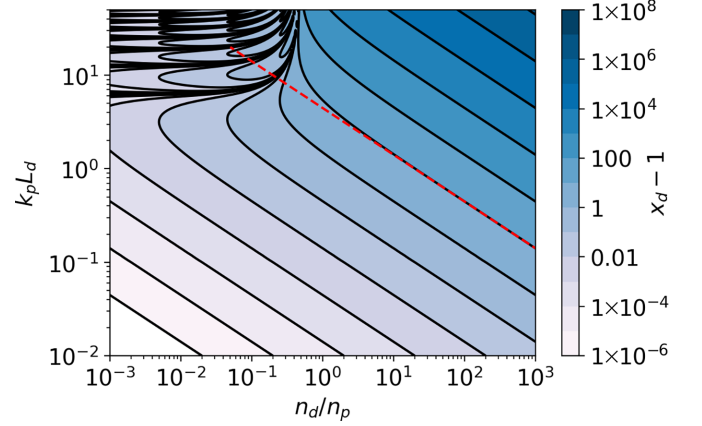


FIG. 1. Dependence of the parameter  $x_d$  on the drive-beam parameters  $k_p L_d$  and  $n_d/n$ . The dashed red line indicates the trajectory a dePWA solution starting at  $(k_p L_d, n_d/n) = (20, 0.0375)$  takes in  $(k_p L_d, n_d/n)$ . The solution is parameterized by the plasma density  $n : 1 \rightarrow 0$ . Note the constancy of  $x_d$  with  $n$  as  $k_p L_d$  gets small or  $n_d/n$  gets large; this is a prediction of the short or high-density (SHD) approximation discussed in Sec. V.

### 1. Low density drive beam: $0 < n_d < n/2$

This is the case studied in Rosenzweig [32]. Here  $x_d$  is a function of an intermediate variable  $\theta_d$  which is determined implicitly as a function of  $L_d$ :

$$(1 - 2n_d/n)k_p L_d = 2[E(\sqrt{2n_d/n}) - E(\theta_d, \sqrt{2n_d/n})], \quad (17a)$$

$$x_d = 1 + \frac{2n_d/n}{1 - 2n_d/n} \cos^2 \theta_d, \quad (17b)$$

$$\text{sgn}(E_{zd}) = \text{sgn} \sin(2\theta_d). \quad (17c)$$

### 2. Drive-beam density equal to background density: $n_d = n/2$

The quantity  $x_d$  is determined implicitly from the equation

$$k_p L_d = \sinh^{-1} \sqrt{x_d - 1} + \sqrt{x_d - 1} \sqrt{x_d}; \quad (18)$$

also,  $\text{sgn}(E_{zd}) = +1$ .

### 3. High-density drive beam: $n_d > n/2$

$x_d$  is a function of  $\theta_d$ , which is implicitly a function of  $n_d$  and  $L_d$ , and  $E_{zd} > 0$ :

$$(2n_d/n - 1)k_p L_d = 2\sqrt{2n_d/n} \times \dots$$

$$(k'^2 F(\theta_d, k) - E(\theta_d, k) + \tan \theta_d \sqrt{1 - k^2 \sin^2 \theta_d}), \quad (19a)$$

$$x_d = 1 + \tan^2 \theta_d, \quad (19b)$$

$$\text{sgn } E_{zd} = +1. \quad (19c)$$

### B. Discussion of wake solutions within driver

In each of the cases  $n_d > n/2$ ,  $n_d = n/2$ , and  $n_d < n/2$ , we can use Eqs. (15) to determine the fluid Lorentz factor  $\gamma$ , the plasma electric field  $E_z$ , and the fluid momentum  $p$  as functions of  $x$  within the driver. The dependence of  $x$  on  $\zeta$  is implicit. In each case, we found the dependence of  $x_d$  and the sign of  $E_{zd}$  on  $n_d$  and  $L_d$ . In Fig. 1, the dependence of  $x_d$  on drive-beam parameters is presented. With  $\gamma_d$ ,  $p_d$ , and  $E_{zd}$ , we

can evaluate the continuity condition for  $\varphi_{st}$  using Eq. (11) as determined in Sec. III.

As discussed by Rosenzweig [32], we know from the continuity of the wake that

$$\gamma_m = \frac{1}{2} \left( \frac{\partial x}{\partial \xi} \Big|_{L_d} \right)^2 + \gamma_d = 1 - \frac{n_d}{n} + \frac{n_d x_d}{n}. \quad (20)$$

If we recall that  $\varphi_d = 1 - x_d$ , we can express the wake amplitude in terms of fluid quantities just as we did  $\varphi_{st}$ . Just as with the other fluid quantities  $\gamma_d$ ,  $p_d$ , and  $E_{zd}$ , we know the potential  $\phi_d$  in terms of  $x_d$  and  $x_d$  implicitly in terms of drive-beam parameters  $n_d, L_d$ . Hence the equation for  $\gamma_m$ ,

$$\gamma_m = 1 - \phi_d n_d / n, \quad (21)$$

is the final equation needed to describe  $\zeta_d$  and  $\frac{\partial \delta n}{\partial \zeta_\delta} \Big|_{\zeta_\delta}$  in terms of the drive-beam parameters.

Using the solutions in this section, we can determine the fluid quantities at the end of the drive beam  $\gamma_d, p_d, E_{zd}$ , and  $\phi_d$  from the drive beam parameters  $n_d, L_d$  and the plasma density  $n(z)$ . We can then calculate  $\varphi_{st}$  and  $\gamma_m$  from the fluid quantities at the end of the drive beam. This map can be used to calculate the wake for any flat-top drive beam and any density  $n$ .

#### IV. OBTAINING PHASE MATCHED DENSITY PROFILE AND FREQUENCY

We found previously that we could determine a plasma density profile that would guarantee phase matching of a laser pulse and the position of positive density gradient in the wake of an electron beam if we could solve the system of Eqs. (4) and (7):

$$\frac{d\omega^2}{dz} \simeq n^{3/2} \sqrt{2[\gamma_m - 1]}, \quad (22)$$

$$\frac{dn}{dz} \simeq \frac{1}{2} \frac{n}{\omega^2} \left[ \frac{d\zeta_\delta}{dn} \right]^{-1}. \quad (23)$$

Using the work in the previous sections, we have maps from the drive-beam parameters  $n_d, L_d$ , and the unperturbed

#### Algorithm 1. Determining the dePWPA wake profile.

- 1: Input: Drive parameters  $n_d, L_d$
- 2: Determine  $x_d$  implicitly from  $n_d, L_d$   $\triangleright$  Equations (A14), (A16), and (A28)
- 3: Evaluate  $\gamma_d, p_d, E_{zd}$ , and  $\phi_d$  as functions of  $x_d$   $\triangleright$  Equations (15)
- 4: Evaluate  $\varphi_{st}$  and  $\gamma_m$  as functions of  $\gamma_d, p_d, E_{zd}$ , and  $\phi_d$   $\triangleright$  Equations (11) and (21)
- 5: Use  $\zeta_d(n)$  to numerically evaluate  $\frac{\partial \zeta_d}{\partial n}$   $\triangleright$  Equation (9)
- 6: Numerically solve  $\frac{d\omega^2}{dz} \simeq n^{3/2} \sqrt{2[\gamma_m - 1]}$ ,  $\frac{dn}{dz} \simeq \frac{1}{2} \frac{n}{\omega^2} \left[ \frac{d\zeta_\delta}{dn} \right]^{-1}$   $\triangleright$  Equations (22) and (23)

plasma density  $n$  to the  $\zeta_\delta$ , the position of positive density gradient where  $\delta n = 0$ , and  $\gamma_m(n; n_d, L_d)$ , the amplitude of the wake behind the drive beam. The function  $\zeta_\delta(n; n_d, L_d)$  can be evaluated and differentiated numerically, yielding values for the gradient  $d\zeta_\delta/dn$ . Thus, we can close the system of Eqs. (22) and (23) and numerically integrate the ordinary differential equations to obtain  $n, \omega$ . We summarize the procedure for obtaining the density profile and frequency shift in Algorithm 1, together with references to the relevant equations in the text. In Fig. 2, we show a sample profile as predicted by Algorithm 1. This computation was performed for a drive beam with density  $n_d = 0.4$ , and length  $L_d = 1$ . The tapered density profile is shown on the left of Fig. 2(a) and the relative gain in frequency,  $\omega/\omega_0$ , is shown on the right of Fig. 2(b). A numerical implementation of the algorithm is shared in Appendix C.

Equations (22) and (23) are a coupled system of differential equations that can be evaluated to determine the density profile and expected frequency shift for phase matched photon acceleration driven by an ultrarelativistic beam driver. However, finding the variation of  $\zeta_\delta$  with density in the nonlinear case is a challenge as it is the solution of an implicit equation. This can be evaluated numerically for specific cases but is not tractable for analytic predictions of long-term behavior or scaling laws. Insight can be gained by using short or

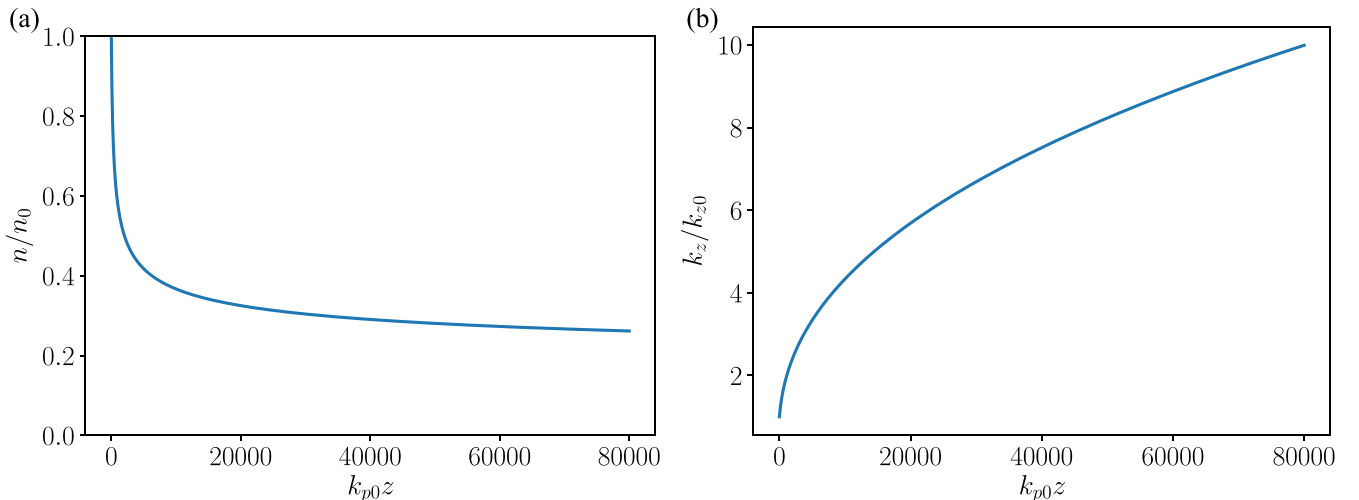


FIG. 2. Numerically determined profiles for unlimited photon acceleration, computed by Algorithm 1 with  $n_d = 0.4, L_d = 1$ , and  $A = 0.4$ . (a) shows the computed plasma density and (b) shows the relative gain in laser frequency.

high-density driver approximations, for which an analytic solution can be found. This is presented in the following section.

### V. SHORT AND HIGH-DENSITY DRIVER LIMITS, UNLIMITED PHOTON ACCELERATION, AND WEAK DRIVER LIMIT

In this section, we consider phase-matched photon acceleration in various limits to explain the pattern seen in Fig. 1, where the parameter  $x_d$  is constant with respect to  $n$  for small  $k_p L_d$  or large  $n_d/n$ . We investigate the plasma response behind the drive beam in both the short and high-density drive-beam limits. In each case, we find  $x_d \simeq 1 + \frac{n_d L_d^2}{2}$ , as indicated in Fig. 1.

#### A. Short drive-beam limit

First, we consider the case  $k_p L_d \ll 1$ . Due to the qualitative distinction between drive beams of density  $n_d/n > 1/2$  and  $n_d/n < 1/2$ , we consider the short drive-beam limit in each case separately.

##### 1. Low-density drive beam: $n_d < n/2$

Recall the equations describing the plasma response behind a low-density beam,  $n_d = n_d/n < 1/2$ , are

$$(1 - 2n_d/n)k_p L_d = 2[E(\sqrt{2n_d/n}) - E(\theta_d, \sqrt{2n_d/n})], \quad (24a)$$

$$x_d = 1 + \frac{2n_d/n}{1 - 2n_d/n} \cos^2 \theta_d, \quad (24b)$$

where  $E(\theta, k) \equiv \int_0^\theta \sqrt{1 - k^2 \sin^2 \theta'} d\theta'$  and  $E(k) \equiv E(\pi/2, k)$ . In the limit  $k_p L_d \ll 1$ , Eq. (24a) becomes

$$E(\sqrt{2n_d/n}) = E(\theta_d, \sqrt{2n_d/n}), \quad (25)$$

meaning  $\theta_d \approx \pi/2$ .

If we then expand around  $\theta_d = \pi/2$  and approximate the integral in Eq. (24a), we find

$$\begin{aligned} E(\sqrt{2n_d/n}) - E(\theta_d, \sqrt{2n_d/n}) \\ \simeq \sqrt{1 - 2n_d/n}(\pi/2 - \theta_d), \end{aligned} \quad (26)$$

and hence  $\theta_d \simeq \pi/2 - \sqrt{1 - 2n_d/n} k_p L_d/2$ . Then  $\cos^2 \theta_d \simeq \frac{1}{4}(1 - 2n_d/n)(k_p L_d)^2$ . In these normalized units,  $k_p = \sqrt{n}$  and thus

$$x_d \simeq 1 + \frac{n_d L_d^2}{2}. \quad (27)$$

##### 2. High-density drive beam: $n_d/n > 1/2$

In this section, we derive the plasma density response behind a high density, meaning  $n_d/n > 1/2$ , short ( $k_p L_d < 1$ ) beam. The governing equations are

$$x_d = 1 + \tan^2 \theta_d, \quad (28a)$$

$$\begin{aligned} (2n_d/n - 1)k_p L_d \\ = 2\sqrt{2n_d/n}(k'^2 F(\theta_d, k) - E(\theta_d, k) \\ + \tan \theta_d \sqrt{1 - k^2 \sin^2 \theta_d}), \end{aligned} \quad (28b)$$

$$k^2 = n/2n_d, \quad k'^2 + k^2 = 1. \quad (28c)$$

It can be shown that the angle  $\theta_d$  tends to 0 as  $k_p L_d \rightarrow 0$ . If we expand in small  $\theta_d$  and approximate the integrals for  $F$  and  $E$ , we get

$$\begin{aligned} \left(\frac{2n_d}{n} - 1\right)k_p L_d \\ = 2\sqrt{\frac{2n_d}{n}} \left[ (1 - k^2) \left( \theta_d + \frac{k^2 \theta_d^3}{4} - \mathcal{O}(\theta_d^5) \right) \right. \\ \left. - \left( \theta_d - \frac{k^2 \theta_d^3}{4} + \mathcal{O}(\theta_d^5) \right) \right] \dots \\ + \left( \theta_d + \frac{\theta_d^3}{3} + \mathcal{O}(\theta_d^5) \right) \left( 1 - \frac{k^2 \theta_d^2}{2} + \mathcal{O}(\theta_d^4) \right). \end{aligned} \quad (29)$$

To lowest order in  $\theta_d$ , this is

$$\theta_d = k_p L_d \sqrt{\frac{n_d}{2n}}. \quad (30)$$

Inserting in the  $x_d$  equation, Eq. (28a), and keeping the lowest order in  $\theta_d$ , we have again

$$x_d \simeq 1 + \frac{n_d L_d^2}{2}. \quad (31)$$

#### B. High-density drive-beam limit

In this section, we derive the plasma density of a very high density ( $n_d/n \gg 1/2$ ) beam. As in the preceding section, describing the short driver limit when  $n_d > n/2$ , Sec. V A 2, the plasma response follows the  $n_d > n/2$  equations, Eqs. (28).

If  $k$  is small, then the integrand of the elliptic function  $F(\theta_d, k)$  simplifies and  $F$  becomes

$$F(\theta_d, k) = \int_0^{\theta_d} \frac{1}{\sqrt{1 - k^2 \sin^2 \varphi}} d\varphi \quad (32)$$

$$\simeq \theta_d \left( 1 + \frac{k^2}{4} \right) - \frac{k^2}{8} \sin 2\theta_d. \quad (33)$$

Similarly,

$$E(\theta_d, k) = \theta_d \left( 1 - \frac{k^2}{4} \right) + \frac{k^2}{8} \sin 2\theta_d. \quad (34)$$

Then Eq. (28b) becomes

$$\begin{aligned} \sqrt{\frac{n_d}{2n}} k_p L_d \simeq k'^2 \left[ \theta_d \left( 1 + \frac{k^2}{4} \right) - \frac{k^2}{8} \sin 2\theta_d \right] \\ \times \left[ \theta_d \left( 1 - \frac{k^2}{4} \right) + \frac{k^2}{8} \sin 2\theta_d \right] \\ + \tan \theta_d \left( 1 - \frac{k^2}{2} \sin^2 \theta_d \right). \end{aligned} \quad (35)$$

To lowest order in  $k$ ,  $\tan \theta_d = \sqrt{\frac{n_d}{2}} L_d$  and

$$x_d \simeq 1 + \frac{n_d L_d^2}{2}. \quad (36)$$

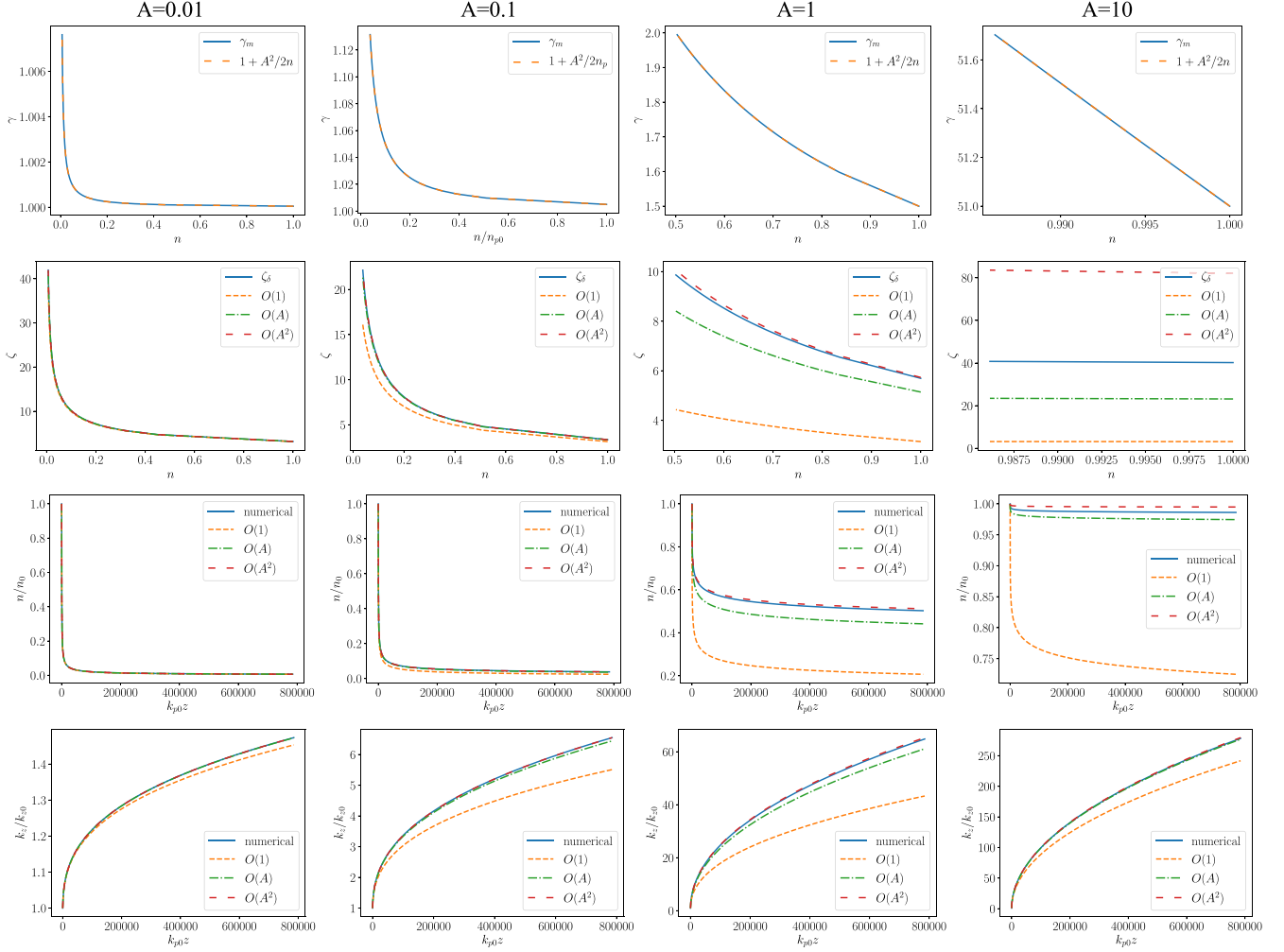


FIG. 3. Comparing numerical and short or high-density small  $A$  expansions. We show that the wake amplitude  $\gamma_m$ , the position of 0 density perturbation  $\zeta_\delta$ , and the predicted density  $n$  and frequency gain  $k_L/k_{L0}$  profiles for  $A = 0.01, 0.1, 1$ , and  $10$  when  $k_{p0}L_{d0} = 0.01$ . The length satisfies  $k_{p0}L_d \ll 1$ , so  $\gamma_m = 1 + A^2/2n$  is always accurate. The expansion to  $\mathcal{O}(A^2)$  is quite accurate for  $\zeta_\delta$ ,  $n$ , and  $k_L$  for  $A$  as large as  $1$ . The expansion when  $A = 10$  is not good for  $\zeta_\delta$  but is surprisingly accurate in predicting  $n$  and  $k_L$  even for  $A = 10$ .

### C. Implications of the short and high-density limits

As long as the drive beam is not both long and low density, the plasma response behind the driver is characterized by  $x_d = 1 + \frac{n_d L_d^2}{2}$ . Then the wake amplitude is  $\gamma_m \simeq 1 + \frac{n_d^2 L_d^2}{2n}$ .

The areal beam charge density  $A \equiv n_d L_d$  is a measure of the strength of the drive beam, especially in the short drive-beam limit. The wake amplitude is

$$\gamma_m = 1 + \frac{A^2}{2n}. \quad (37)$$

Hence, the frequency shift relation, Eq. (22), in the short or high-density limit is

$$\frac{d\omega^2}{dz} = nA. \quad (38)$$

Equations (38) and (23) may be combined,

$$\frac{d\omega^2}{dz} = \frac{d\omega^2}{dn} \frac{dn}{dz} = 2A\omega^2 \frac{d\zeta_\delta}{dn}, \quad (39)$$

and directly integrated,

$$\int_{\omega_0}^{\omega} \frac{1}{\omega'^2} d\omega' = 2A \int_{n_0}^n \frac{d\zeta_\delta}{dn'} dn', \quad (40)$$

to obtain

$$\omega(n) = \omega_0 \exp[A(\zeta_\delta(n) - \zeta_{\delta 0})], \quad (41)$$

defined for  $n$  in  $(0, n_0]$  where  $n(0) = n_0$ .

The matched phase in the wake,  $\zeta_\delta$ , also has a simpler expression in the SHD approximation. Since the width of the beam vanishes, the wake starts at phase  $\varphi_0 = \pi/2$  and the expression for  $\zeta_\delta$  is

$$\begin{aligned} \zeta_\delta &= \zeta(3\pi/2) - \zeta(\pi/2) \\ &= \frac{1}{\omega_p} \left[ \frac{4}{\kappa'} E(\kappa) - 2\kappa' K(\kappa) + 4 \frac{\kappa}{\kappa'} \right], \end{aligned} \quad (42)$$

where  $\kappa^2 = (1 + 4n/A^2)^{-1}$  and  $\kappa'^2 = (1 + A^2/4n)^{-1}$ .

Larger frequency shifts require lower densities and longer propagation distances. For a given frequency  $\omega$  to be realized, Eq. (41) indicates what plasma density  $n$  must be attained.

Then the propagation distance  $z$  can be determined as a function of  $n$ . The differential relation between  $z$  and  $n$  is

$$\frac{dz}{dn} = \frac{d\omega^2}{dn} \frac{dz}{d\omega^2} = \frac{2\omega^2}{n} \frac{d\zeta_\delta}{dn}. \quad (43)$$

This equation can be integrated to give

$$z = 2\omega_0^2 \int_{n_0}^n \frac{1}{n'} \frac{d\zeta_\delta}{dn'} e^{2A(\zeta_\delta(n) - \zeta_{\delta 0})} dn'. \quad (44)$$

Equations (41) and (44) provide a complementary and more analytic method of determining density profiles and frequency shifts to the numerical integration of Eqs. (22) and (23).

#### D. Unlimited photon acceleration

Since  $d\omega^2/dz > 0$  and  $dn/dz < 0$ , there are no fixed points or periodic orbits and so, by the Poincaré-Bendixon theorem, there are no limit sets to the orbits. In fact, we demonstrate that as  $n \rightarrow 0$ ,  $\zeta_\delta(n) \rightarrow \infty$  and  $\omega(n) \rightarrow \infty$ .

Recall that  $\kappa^2 = \frac{A^2}{4n+A^2} \rightarrow 1$  as  $n \rightarrow 0$  and so  $\kappa'^2 \rightarrow 0$ . It can be shown [41] that  $E(\kappa) \rightarrow 1$  as  $\kappa \rightarrow 1$  and

$$K(\kappa) \sim \ln \frac{4}{\kappa'} \quad \text{as } \kappa \rightarrow 1. \quad (45)$$

Now  $\zeta_\delta$  simplifies to

$$\begin{aligned} \zeta_\delta &\sim \frac{1}{\sqrt{n}} \left[ \frac{4}{\kappa'} (1+1) - 2\kappa' \ln \frac{4}{\kappa'} \right] \\ &\sim \frac{1}{\sqrt{n}} \frac{8}{\kappa'} \rightarrow \infty \quad \text{as } n \rightarrow 0. \end{aligned} \quad (46)$$

From Eq. (41), the laser frequency  $\omega$  is unbounded as plasma density tends to 0. This unlimited photon acceleration (see also Bulanov *et al.* [22] for some discussion of unlimited particle acceleration) is quite significant in that a physical mechanism for frequency shift is now rigorously proven to admit arbitrary frequency shifts, provided that the drive beam can be sustained. This unlimited photon acceleration is, however, only true within the idealization of the mathematical model. See Appendix B for a discussion on limitations due to nonideal conditions.

#### E. Weak driver limit

For a moderate strength driver,  $A < 1$ , the function  $\zeta(n)$  is

$$\omega_p \zeta = \varphi - \frac{A}{n^{1/2}} \sin \varphi + \frac{A^2}{16n} (3\varphi + \sin 2\varphi). \quad (47)$$

The location of the zero density perturbation,  $\zeta_\delta$ , can be described accurately by the expansion

$$\zeta_\delta = \frac{\pi}{n^{1/2}} + \frac{2A}{n} + \frac{3\pi}{16} \frac{A^2}{n^{3/2}} + \dots \quad (48)$$

Retaining up to the third term in this expansion, the phase-matching relation, Eq. (23), is

$$\frac{dn}{dz} = -\frac{n^{5/2}}{\pi\omega^2} \left( 1 + \frac{4\pi A}{n^{1/2}} + \frac{9A^2}{16n} \right)^{-1}. \quad (49)$$

The expansions developed in this section are seen to be accurate over a large parameter range. In Fig. 3, we present  $\gamma_m$ ,  $\zeta_d$ ,  $n$ , and  $k_L$  for  $A = 0.01, 0.1, 1$ , and  $10$  and for  $L_{d0} = 0.01$ . This short driver length guarantees that the SHD limit holds

very well. This is why the dashed and solid lines in the top row, which shows the wake amplitude  $\gamma_m$ , agree so well for all  $A$ . The second row shows the position of 0 density perturbation  $\zeta_\delta$  and its approximations, which agree with the exact function to  $A = 1$ . The next rows show the predicted density profile and frequency gain. The density profile is accurately predicted with the expansion for  $A$  as large as 1. The slow variation in  $n$  in all cases means that the predicted frequency gain of the analytic expansion matches the numerical prediction for all values of  $A$  calculated. We see that generally the expansion is good for  $A = 1$  and surprisingly accurate even for  $A = 10$ .

## VI. CONCLUSIONS

In conclusion, we have given the details for an analytic model for a plasma density profile that achieves phase matching for a beam driven plasma wakefield accelerator. The model predicts arbitrary frequency shift limited only by depletion of the drive beam. This model was used to generate the density profiles used in Ref. [31] that were used in *ab initio* relativistic electromagnetic particle-in-cell simulations. The simulations in that paper were both one- and three-dimensional; the one-dimensional solutions were demonstrated to be effective in three dimensions in the broad-driver regime, as expected. The algorithm developed should enable other researchers to easily study the dePWPA scheme.

## ACKNOWLEDGMENTS

This work was supported by Air Force Office of Scientific Research (AFOSR) Grant No. FA9550-19-1-0072 and US National Science Foundation (NSF) Grant No. 1804463. Computational resources were provided by Advanced Research Computing at the University of Michigan. The authors acknowledge the OSIRIS Consortium, consisting of UCLA and IST (Lisbon, Portugal) for providing access to the OSIRIS 4.0 framework.

## APPENDIX A: DETAILS OF THE SOLUTION FOR THE WAKE WITHIN THE DRIVER

In this Appendix, we determine the map from drive-beam parameters to wake behind the driver. In the previous section, we found that the wake behind the driver can be completely understood in terms of its amplitude  $\gamma_m$  and a continuity condition between the wake within the drive beam and the wake behind the drive beam. The continuity condition depends on the plasma particle Lorentz factor  $\gamma_d$ , momentum  $p_d$ , and electric field  $E_{zd}$  at the end of the drive beam. In this Appendix, we derive  $\gamma_m$ ,  $\gamma_d$ ,  $p_d$ , and  $E_{zd}$  in terms of the drive-beam parameters. To determine the wake quantities at the end of the drive beam, we solve the fluid equations with nonzero drive-beam density.

This section consists of three parts. First, the plasma fluid equations within the drive beam are presented. Next, these are solved in three cases depending on the relation between the drive-beam density  $n_d$  and the unperturbed plasma density  $n = n(z)$ , namely, when  $n_d > n/2$ ,  $n_d = n/2$ , and  $n_d < n/2$ . Since there are three solution sets, the quantities  $\gamma_d$ ,  $p_d$ , and  $E_{zd}$  are expressed in three different cases. The electric

potential at the end of the driver,  $\phi_d$ , will also be presented in each case, since it is needed for determining the amplitude  $\gamma_m$  of the wake behind the driver. This Appendix ends by deriving the relation  $\gamma_m = 1 - n_d \phi_d$  between the drive-beam parameters and the amplitude of the wake behind the driver.

We begin with the plasma fluid equations within the drive beam. We assume an ultrarelativistic ( $\beta_d \rightarrow 1$ ) drive beam, in which case the fluid equations are

$$\frac{n_w}{n} = \frac{1}{1 - \beta}, \quad (\text{A1a})$$

$$\frac{1}{\omega_p^2} \frac{\partial^2}{\partial \zeta^2} (\gamma(1 - \beta)) = \frac{\beta}{1 - \beta} + \frac{n_d}{n}. \quad (\text{A1b})$$

Using the approximation that the plasma density  $n(z)$  is slowly varying, we may use the wake solutions in constant density to find  $n_w(\zeta; n(z))$ . We therefore treat  $n(z)$  as a constant,  $n$ , and write  $\zeta = \omega_p \zeta$ ,  $n_d = n_d/n$ , and  $L_d = \omega_p L_d/c$ . This normalization was not used in the text to prevent confusion when incorporating the variation of  $n(z)$ . Here, however, in the context of determining the wake profile, the constant density assumption permits the convenient suppression of  $n$ .

Following Rosenzweig [32], we let

$$x(\zeta) \equiv \gamma(1 - \beta) = \sqrt{\frac{1 - \beta}{1 + \beta}}. \quad (\text{A2})$$

This leads to

$$\frac{\partial^2 x}{\partial \zeta^2} = \frac{1}{2} \left( \frac{1}{x^2} - 1 + 2n_d \right). \quad (\text{A3})$$

We assume that the plasma is quiescent ahead of the driver, so for  $\zeta \leq 0$ ,  $\beta = 0 = p = E$ , and  $n = 1 = \gamma = x$ .

This integrates once to give

$$\left( \frac{\partial x}{\partial \zeta} \right)^2 = 2(1 - n_d) - 1/x + (2n_d - 1)x. \quad (\text{A4})$$

We make a detour to discuss the electric field and choice of sign for the square root that equals  $\frac{\partial x}{\partial \zeta}$ . Recall that Gauss's law in this ultrarelativistic problem states

$$-\frac{1}{v_d} \frac{\partial E_z}{\partial \zeta} = 4\pi e(n_i - n_e - n_d),$$

$$\frac{\partial E_z}{\partial \zeta} = -(1 - n_w - n_d) = \frac{\partial^2 x}{\partial \zeta^2}. \quad (\text{A5})$$

We can make the identifications  $E_z = \pm \frac{\partial x}{\partial \zeta}$  and  $\phi = \pm(-x + 1)$  since  $E_z = 0 = \frac{\partial x}{\partial \zeta}$  for  $\zeta \leq 0$ . Since we made the assumption that the plasma species and beam particles are electrons, immediately behind the driver the electron density is decreased; then  $\frac{\partial E_z}{\partial \zeta} = n_w + n_d - 1 > 0$  and we start with the positive square root for  $\frac{\partial x}{\partial \zeta}$ .

For identifying dependence of fluid quantities on drive beam parameters, we identify dependence on  $x$ :

$$\gamma = \frac{1 + x^2}{2x}, \quad (\text{A6a})$$

$$p = \frac{1 - x^2}{2x}, \quad (\text{A6b})$$

$$E_z = \frac{\partial x}{\partial \zeta} = \text{sgn}(E_z) \sqrt{2(1 - n_d) - 1/x + (2n_d - 1)x}, \quad (\text{A6c})$$

$$\phi = 1 - x. \quad (\text{A6d})$$

The sign of  $E_z$  can change in some cases; we comment in each case whether  $E_z$  stays positive or not and how to determine the sign of  $E_{zd}$ .

In Eq. (A4), the term  $(2n_d - 1)x$  changes signs based on the relation of  $n_d$  and  $1/2$ , as does the qualitative behavior of the solution and the technique used to derive the solution. There are three cases to consider:

### 1. $0 < n_d < 1/2$

This is the case studied in Rosenzweig [32]; the equation for  $x$  is

$$\frac{\partial x}{\partial \zeta} = \sqrt{2 - 2n_d - 1/x - (1 - 2n_d)x}. \quad (\text{A7})$$

Following Rosenzweig, we perform a change of variables to

$$(x - 1)(1 - 2n_d) \equiv 2n_d \cos^2 \theta \quad (\text{A8})$$

and write the solution as an implicit relation for  $\theta$  as a function of  $\zeta$ :

$$(1 - 2n_d)\zeta(\theta) = 2(E(\sqrt{2n_d}) - E(\sqrt{2n_d}, \theta)), \quad (\text{A9})$$

where

$$E(\theta, k) \equiv \int_0^\theta \sqrt{1 - k^2 \sin^2 \theta'} d\theta' \quad (\text{A10})$$

is the incomplete elliptic integral of the second kind and  $E(k) = E(\pi/2, k)$  is the corresponding complete integral of the second kind.

The above relation is valid within the driver for  $-L_d \leq \zeta \leq 0$ . Solving for  $\theta(\zeta)$ , we can find  $x$ :

$$x(\zeta) = 1 + \frac{2n_d}{1 - 2n_d} \cos^2 \theta(\zeta). \quad (\text{A11})$$

Here  $x(\zeta)$  is oscillatory, so determining the electric field requires determining sign changes. Since the electric field is equal to  $\pm \frac{\partial x}{\partial \zeta}$ ,  $\frac{\partial x}{\partial \theta} = \frac{2n_d}{1 - 2n_d} \sin 2\theta(\zeta)$ , and

$$\frac{\partial \theta}{\partial \zeta} = \frac{2n_d - 1}{2\sqrt{1 - n_d} \sin^2 \theta} > 0, \quad (\text{A12})$$

we know that

$$\text{sgn}(E_z) = \text{sgn} \sin 2\theta. \quad (\text{A13})$$

In summary,  $x_d$  is a function of an intermediate variable  $\theta_d$  which is determined implicitly from the following equations:

$$(1 - 2n_d)L_d = 2(E(\sqrt{2n_d}) - E(\theta_d, \sqrt{2n_d})), \quad (\text{A14a})$$

$$x_d = 1 + \frac{2n_d}{1 - 2n_d} \cos^2 \theta_d, \quad (\text{A14b})$$

$$\text{sgn}(E_{zd}) = \text{sgn} \sin(2\theta_d). \quad (\text{A14c})$$

### 2. $n_d = 1/2$

In this case, the equation for  $x$  simplifies to

$$\frac{\partial x}{\partial \zeta} = \sqrt{1 - \frac{1}{x}}. \quad (\text{A15})$$

Since  $\frac{\partial \zeta}{\partial x} > 0$  at  $x = 1$ ,  $\zeta = 0$ ,  $\frac{\partial x}{\partial \zeta} > 0$  for all  $\zeta$  and so  $x(\zeta)$  is a positive, monotonically increasing function. In addition, as  $x(\zeta)$  is nonoscillatory,  $E_z$  and  $n_w$  will be monotone and, in particular,  $E_z$  stays positive within the drive beam. Similarly, the electric potential  $\phi < 0$  within the drive beam.

The quantity  $x_d$  is determined implicitly from the equation

$$L_d = \sinh^{-1} \sqrt{x_d - 1} + \sqrt{x_d - 1} \sqrt{x_d} \quad (\text{A16})$$

and  $\text{sgn}(E_{zd}) = +1$ .

### 3. $n_d > 1/2$

The equation for  $x$  is

$$\frac{\partial x}{\partial \zeta} = \sqrt{2(1 - n_d) - 1/x + (2n_d - 1)x}. \quad (\text{A17})$$

Note that this will stay positive, so  $x$  is a positive, monotonically increasing function of  $\zeta$ . Rearranging so we can solve for  $\zeta(x)$ ,

$$\frac{\partial \zeta}{\partial x} = \frac{\sqrt{x}}{\sqrt{x - (2n_b - 1)x - 1 + (2n_b - 1)x^2}}, \quad (\text{A18})$$

and integrating, we have

$$\sqrt{2n_d - 1} \int_0^\zeta d\zeta' = \int_1^x \frac{\sqrt{x'}}{\sqrt{(x' - 1)(x' + \frac{1}{2n_d - 1})}} dx'. \quad (\text{A19})$$

Following a similar vein to the solution technique for  $n_d < 1/2$ , we use the substitution

$$(x - 1)(2n_d - 1) = t^2, \quad (\text{A20})$$

and arrive at

$$\sqrt{2n_d - 1} \zeta = \frac{2}{\sqrt{2n_d - 1}} \int_0^t \frac{\sqrt{t^2 + 2n_d - 1}}{\sqrt{t^2 + 2n_d}} dt. \quad (\text{A21})$$

The integral in Eq. (A21) is an elliptic integral. We find a recipe for its evaluation in Eqs. (221.04) and (313.02) of Byrd and Friedman [41]:

$$\begin{aligned} & \int_0^t \frac{\sqrt{t'^2 + b^2}}{\sqrt{t'^2 + a^2}} dt' \\ &= gb^2 \left( \frac{1}{k^2} \left\{ k^2 F \left( \tan^{-1} \frac{t}{b}, k \right) - E \left( \tan^{-1} \frac{t}{b}, k \right) \right. \right. \\ & \quad \left. \left. + \frac{t}{b} \sqrt{1 - k^2 \sin^2 \left( \tan^{-1} \frac{t}{b} \right)} \right\} \right), \quad (\text{A22}) \end{aligned}$$

$$\begin{aligned} a^2 &= 2n_d, & b^2 &= 2n_d - 1, & g &= \frac{1}{a} = \frac{1}{\sqrt{2n_d}}, \\ k^2 &= \frac{a^2 - b^2}{a^2} = \frac{1}{2n_d}, & k'^2 &= 1 - k^2 = \frac{2n_d - 1}{2n_d}. \quad (\text{A23}) \end{aligned}$$

Now we employ a trigonometric substitution,

$$\tan \theta = \frac{t}{b}, \quad (\text{A24})$$

and, observing that

$$\frac{gb^2}{k^2} = \frac{2n_d - 1}{\sqrt{2n_d}} \frac{2n_d}{2n_d - 1} \quad (\text{A25})$$

$$= \sqrt{2n_d}, \quad (\text{A26})$$

we arrive at

$$\begin{aligned} (2n_d - 1)\zeta &= 2\sqrt{2n_d} \times \dots \\ & (k'^2 F(\theta, k) - E(\theta, k) \\ & \quad + \tan \theta \sqrt{1 - k^2 \sin^2 \theta}). \quad (\text{A27}) \end{aligned}$$

To complete the  $n_d > n/2$  equations, we combine the substitutions in Eqs. (A20) and (A24) to get the equation for  $x_d$  as a function of  $\theta_d$  and include the condition on  $\text{sgn} E_{zd}$ :

$$x_d = 1 + \tan^2 \theta_d, \quad (\text{A28a})$$

$$\text{sgn} E_{zd} = +1. \quad (\text{A28b})$$

To evaluate the accuracy of this map in each of the three cases, we compare the theoretical wake profile with the wake profile computed in 1D PIC simulations for drive beams of various lengths and of densities at, greater than, and less than the plasma densities. As seen in Fig. 4, the theoretical prediction agrees very well with the computed wake.

## APPENDIX B: LIMITATIONS TO THE IDEAL 1D MODEL

The mathematical 1D dePWA model assumes an ultra-relativistic driver moving at the speed of light. Given these assumptions, the frequency shift is arbitrarily large (unlimited). In practice, these assumptions are violated and this imposes some limitations on the frequency shift that is realizable. We discuss some of these limitations in this Appendix.

The treatment of the wake behind the drive beam as an AP wave assumes a cold 1D plasma and that  $\gamma_m < \gamma_d$ ; if this condition is not met, the AP wave breaks. Background plasma particles can be trapped in the wake, the fields and density profile are altered, and, in particular, the plasma density gradient differs from the AP model. Wave breaking is not considered in this paper but would limit the achievable frequency shift. For the ultrarelativistic drive-beam approximation assumed in our work,  $v_d \rightarrow c$ , the Lorentz factor  $\gamma_d \rightarrow \infty$  and the AP condition is always met. Given a realistic driver with  $v_d < c$ , the AP wave breaks when  $\gamma_m \geq \gamma_d$ . Consider, for example, a 10 GeV electron beam driver for which  $\gamma_d \approx 20\,000$ , with normalized areal beam charge density  $A \sim 1$ . In this case, using the ultrashort beam limit described above for  $\gamma_m$ , the wave-breaking condition occurs when  $20\,000 = 1 + A^2/2n$ , so the limit can be estimated using  $A^2/n \sim 10^4$ , i.e.,  $n$  would drop to  $10^{-4}$  of its initial value. Hence, the plasma frequency would drop to  $10^{-2}$  of its initial value and the relativistic plasma wavelength would increase by a factor  $\mathcal{O}(100)$ . Now recall the frequency shift scaling from Eq. (41),  $\omega(n) = \omega_0 \exp(A(\zeta_\delta(n) - \zeta_{\delta 0}))$ . The position of the laser,  $\zeta_\delta$ , scales with the plasma wavelength. We can therefore estimate that wave breaking occurs for these parameters when the laser frequency has increased by a factor of  $\exp(\mathcal{O}(100))$ ; wave breaking is evidently not a very restrictive limit in the cold 1D model.

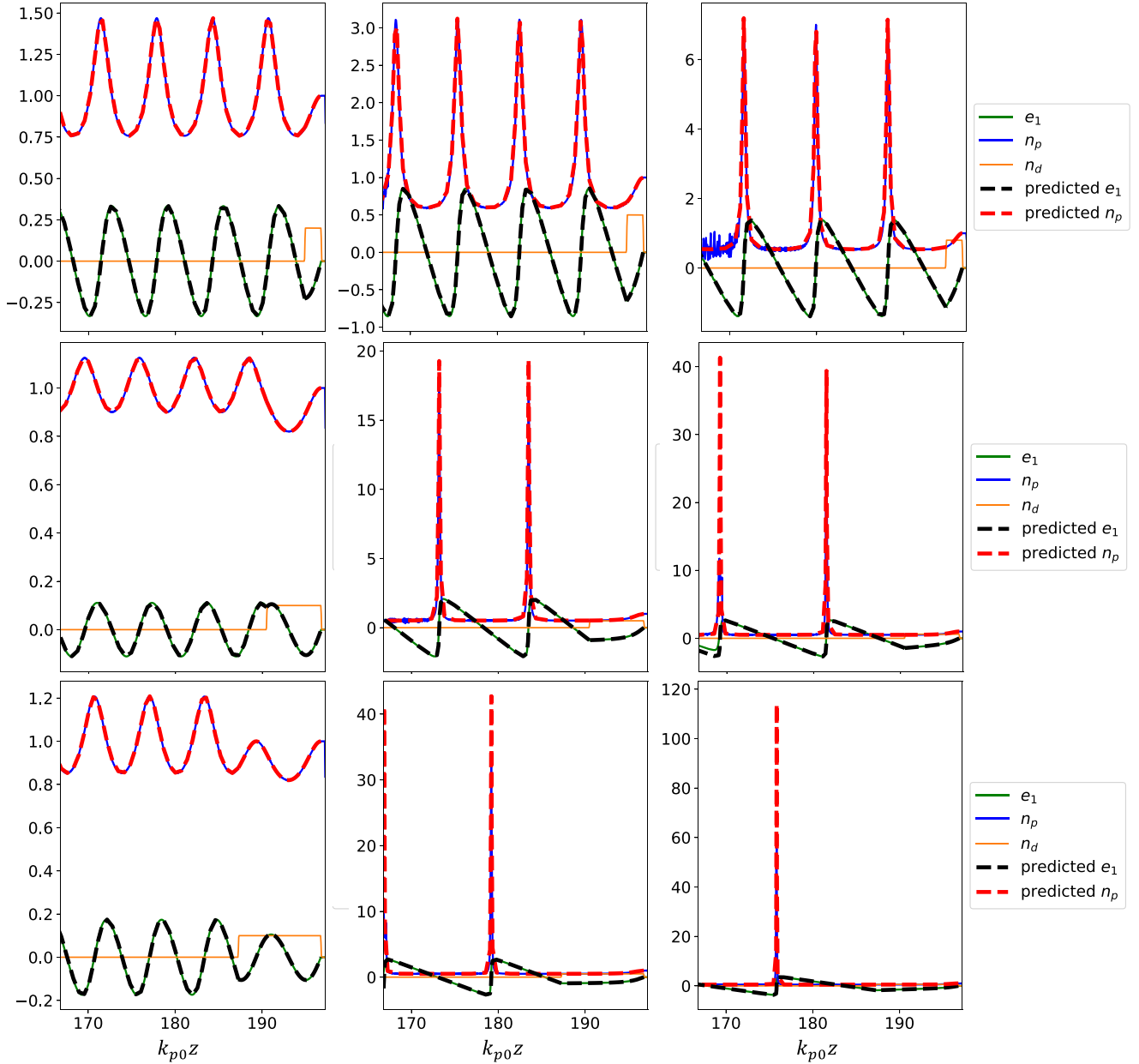


FIG. 4. Analytic expressions in the wake compared to OSIRIS 1D simulation data. Top row:  $k_{p0}L_{d0} = 1.9$ ,  $n_{d0}/n = 0.2, 0.5, 0.8$ . Middle row:  $k_{p0}L_{d0} = 6.28$ ,  $n_{d0}/n = 0.1, 0.5, 0.6$ . Bottom row:  $k_{p0}L_{d0} = 9.5$ ,  $n_{d0}/n = 0.1, 0.5, 0.6$ . The expressions are exact in a uniform density plasma (here  $n = 1$  but any value of  $n$  is possible).

On the other hand, it is well-known [42] that the wave-breaking threshold is lowered by finite plasma temperature. Including the effect of finite plasma temperature may more significantly limit the achievable frequency shift and would be an interesting direction of future work. More importantly, for experimental realization of dePWPA, transverse motion and 3D effects were also not considered in this paper. Although we showed in our previous paper [31] that, in practice, the 1D solutions could be used reasonably in the 3D case, inclusion of transverse effects introduces additional wave-breaking mechanisms and qualitative changes to the wake profile that would affect the asymptotic limits presented here. For example, if the plasma is driven hard enough that the plasma electrons

can be completely expelled from the wake, it may form a spherical cavity of positive charge behind the driver, known as the blowout [43] or bubble [44] regime. In the blowout regime, the smoothly varying plasma gradient becomes very steep in a narrow sheath region around the bubble. While this steep gradient may provide enhanced photon acceleration, the laser pulse is likely to be much longer than the scale length of the density gradient and may not be well modeled by the dePWPA scheme presented in this paper. Moreover, the size of the wake and, particularly, the position  $\zeta_s$  are different in the blowout regime than in the 1D PA wave. Several 3D wakefield models for the bubble regime have been put forward in the literature that agree well with PIC simulation results [45–47];

```
[1]: import numpy as np
import matplotlib as mpl
from matplotlib import pyplot as plt
import dephasingless_pwpa_plasma_profile as depa

[2]: nc0_np0 = 100
nd0_np0 = 0.2
kp0Ld0 = 1.9
lambda_L0 = 8e-7
lambda_p0 = lambda_L0 * np.sqrt(nc0_np0)
kp0 = 2*np.pi / lambda_p0
kp0z, n_n0_depa, k_kp0_depa = depa.get_depa_profile(nc0_np0,
                                                    nd0_np0,
                                                    kp0Ld0,
                                                    kp0z_final=80000,
                                                    n_steps=160001)

[4]: mpl.rcParams.update({'font.size': 18})

[5]: fig, axT = plt.subplots(1,2,figsize=(10,4.5))
ax = axT[0]
ax.plot(kp0z, n_n0_depa)
ax.set_xlabel(r'$\omega_{p0}t=k_{p0}z$')
ax.set_ylabel(r'$n/n_0$')
ax2 = ax.twinx()
ax2.plot(kp0z/kp0, n_n0_depa)
ax2.set_xlabel(r'$z$ [m] (assume $\lambda_{L0}=800$ {\rm nm}$)')
ax = axT[1]
ax.plot(kp0z, np.sqrt(k_kp0_depa/k_kp0_depa[0]))
ax.set_xlabel(r'$\omega_{p0}t=k_{p0}z$')
ax.set_ylabel(r'$k/k_0$')
ax2 = ax.twinx()
ax2.plot(kp0z/kp0, np.sqrt(k_kp0_depa/k_kp0_depa[0]))
ax2.set_xlabel(r'$z$ [m] (assume $\lambda_{L0}=800$ {\rm nm}$)')
plt.tight_layout()
```

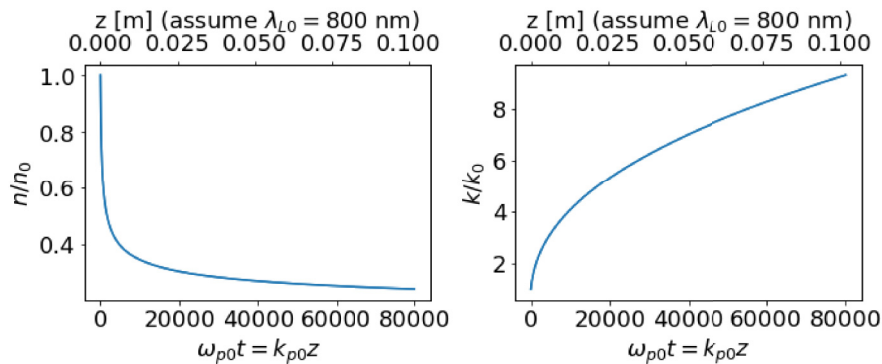


FIG. 5. Jupyter notebook output demonstrating usage of the Python code `dephasingless_pwpa_plasma_profile` to calculate the dephasingless PWPA plasma density profile and theoretical laser frequency.

it would be interesting to investigate whether the dePWPA theory can be extended to include the 3D nonlinear model of the blowout in calculating  $\zeta_\delta$  and  $d\zeta_\delta/dn$  and whether photon acceleration can still be effective in the blowout regime.

Laser-driven dephasingless photon acceleration, a deLWPA scheme, would be of interest. The evolution of a laser pulse is very different from an electron beam, so LWPA theoretically is a separate research topic. However, there are spatiotemporal pulse-shaping techniques (that generate a

```

In [6]: 1 help(depa.get_depa_profile)
Help on function get_depa_profile in module dephasingless_pwpa_plasma_profile:

get_depa_profile(nc0_np0, nd0_np0, kp0Ld0, n_n0_min=0.01, n_n0_max=1.1, kp0z_initial=0, kp0z_final=50000, n_steps=100001)
Calculate the dephasingless plasma wakefield photon acceleration
(dePWPA) plasma density profile and theoretical laser frequency

Parameters
-----
nc0_np0: float, ratio of initial laser critical density to plasma density
or ratio of laser frequency squared to plasma frequency squared
nd0_np0: float, ratio of initial drive beam density to initial plasma density
kp0Ld0: float, drive beam length normalized to initial plasma wavenumber
n_n0_min: minimum possible plasma density ratio that can be computed
n_n0_max: maximum possible plasma density ratio that can be computed
kp0z_initial: float, start time/position of dePWPA profile
kp0z_final: float, final time/position of dePWPA profile
n_steps: number of integration steps in numerical solving of the dePWPA
coupled differential equations

Returns
-----
kp0z : numpy array

```

FIG. 6. A sample help message for the `get_depa_profile` function in the `dephasingless_pwpa_plasma_profile` Python code.

so-called flying focus), that would enable a laser pulse with group velocity that mimics the rigid motion of an ultrarelativistic electron beam driver [48,49]. In this case, we anticipate that minor modifications to the dePWPA theory would accommodate similar frequency shifts driven by a laser pulse with flying focus, similar to previous work using an ionization front [23].

### APPENDIX C: EXAMPLE CODE TO OBTAIN PLASMA DENSITY PROFILE

In this Appendix, we present the practical evaluation of the dephasingless PWPA plasma density profile using a Python script. A sample Jupyter notebook is shown in Fig. 5, demonstrating usage of the code along with a visualization of the resulting plasma density profile and laser frequency. To use

this code to generate a plasma density profile in the Python-based PIC code FBPIC, we created an interpolating function based on the arrays returned by the Python dePWPA code. To generate a profile for the OSIRIS PIC code, the plasma density profile must be expressed in terms of elementary functions that are recognized by the OSIRIS function parser. We found that a function of the form  $f(x) = a + b/(c + x)^d$  yielded a good fit for the plasma density profile.

The Python code itself, `dephasingless_pwpa_plasma_profile`, is provided in the Supplemental Material [33]. The primary function in `dephasingless_pwpa_plasma_profile` is `get_depa_profile`, which takes as required input the initial critical-to-plasma-density ratio, the initial drive beam density, and the initial drive beam length and returns arrays of propagation distances, the plasma density profile at those distances, and the theoretical resulting frequency shift. This code is documented for ease of use, as shown in Fig. 6.

- 
- [1] J. Rossbach, J. R. Schneider, and W. Wurth, Ten years of pioneering x-ray science at the free-electron laser flash at DESY, *Phys. Rep.* **808**, 1 (2019).
  - [2] M. A. Khokhlova and V. V. Strelkov, Highly efficient XUV generation via high-order frequency mixing, *New J. Phys.* **22**, 093030 (2020).
  - [3] Z. Chang, A. Rundquist, H. Wang, M. M. Murnane, and H. C. Kapteyn, Generation of coherent soft x rays at 2.7 nm using high harmonics, *Phys. Rev. Lett.* **79**, 2967 (1997).
  - [4] S. V. Bulanov, T. Esirkepov, and T. Tajima, Light intensification towards the Schwinger limit, *Phys. Rev. Lett.* **91**, 085001 (2003).
  - [5] M. Kando, A. S. Pirozhkov, K. Kawase, T. Z. Esirkepov, Y. Fukuda, H. Kiriya, H. Okada, I. Daito, T. Kameshima, Y. Hayashi, H. Kotaki, M. Mori, J. K. Koga, H. Daido, A. Y. Faenov, T. Pikuz, J. Ma, L. M. Chen, E. N. Ragozin, T. Kawachi *et al.*, Enhancement of photon number reflected by the relativistic flying mirror, *Phys. Rev. Lett.* **103**, 235003 (2009).
  - [6] S. V. Bulanov, T. Z. Esirkepov, and M. Kando, Relativistic mirrors in plasmas. Novel results and perspectives, *Phys. Usp.* **56**, 429 (2013).
  - [7] B. R. Benware, C. D. Macchietto, C. H. Moreno, and J. J. Rocca, Demonstration of a high average power tabletop soft x-ray laser, *Phys. Rev. Lett.* **81**, 5804 (1998).
  - [8] S. C. Wilks, J. M. Dawson, W. B. Mori, T. Katsouleas, and M. E. Jones, Photon accelerator, *Phys. Rev. Lett.* **62**, 2600 (1989).
  - [9] J. T. Mendonca, *Theory of Photon Acceleration* (Institute of Physics Publishing, Bristol, UK, 2001).
  - [10] W. Mori, The physics of the nonlinear optics of plasmas at relativistic intensities for short-pulse lasers, *IEEE J. Quantum Electron.* **33**, 1942 (1997).
  - [11] T. Esirkepov, S. V. Bulanov, M. Yamagiwa, and T. Tajima, Electron, positron, and photon wakefield acceleration: Trapping, wake overtaking, and ponderomotive acceleration, *Phys. Rev. Lett.* **96**, 014803 (2006).
  - [12] E. Esarey, G. Joyce, and P. Sprangle, Frequency up-shifting of laser pulses by copropagating ionization fronts, *Phys. Rev. A* **44**, 3908 (1991).
  - [13] L. Oliveira e Silva and J. T. Mendonca, Photon acceleration in superluminous and accelerated ionization fronts, *IEEE Trans. Plasma Sci.* **24**, 316 (1996).
  - [14] M. R. Shcherbakov, K. Werner, Z. Fan, N. Talisa, E. Chowdhury, and G. Shvets, Photon acceleration and tunable

- broadband harmonics generation in nonlinear time-dependent metasurfaces, *Nat. Commun.* **10**, 1345 (2019).
- [15] J. M. Dias, C. Stenz, N. Lopes, X. Badiche, F. Blasco, A. Dos Santos, L. Oliveira e Silva, A. Mysyrowicz, A. Antonetti, and J. T. Mendonça, Experimental evidence of photon acceleration of ultrashort laser pulses in relativistic ionization fronts, *Phys. Rev. Lett.* **78**, 4773 (1997).
- [16] C. W. Siders, S. P. Le Blanc, D. Fisher, T. Tajima, M. C. Downer, A. Babine, A. Stepanov, and A. Sergeev, Laser wake-field excitation and measurement by femtosecond longitudinal interferometry, *Phys. Rev. Lett.* **76**, 3570 (1996).
- [17] C. D. Murphy, R. Trines, J. Vieira, A. J. W. Reitsma, R. Bingham, J. L. Collier, E. J. Divall, P. S. Foster, C. J. Hooker, A. J. Langley, P. A. Norreys, R. A. Fonseca, F. Fiuza, L. O. Silva, J. T. Mendonça, W. B. Mori, J. G. Gallacher, R. Viskup, D. A. Jaroszynski, S. P. D. Mangles *et al.*, Evidence of photon acceleration by laser wake fields, *Phys. Plasmas* **13**, 033108 (2006).
- [18] M. R. Edwards, K. Qu, Q. Jia, J. M. Mikhailova, and N. J. Fisch, Cascaded chirped photon acceleration for efficient frequency conversion, *Phys. Plasmas* **25**, 053102 (2018).
- [19] Z. Nie, C. H. Pai, J. Hua, C. Zhang, Y. Wu, Y. Wan, F. Li, J. Zhang, Z. Cheng, Q. Su, S. Liu, Y. Ma, X. Ning, Y. He, W. Lu, H. H. Chu, J. Wang, W. B. Mori, and C. Joshi, Relativistic single-cycle tunable infrared pulses generated from a tailored plasma density structure, *Nat. Photon.* **12**, 489 (2018).
- [20] E. Esarey, A. Ting, and P. Sprangle, Frequency shifts induced in laser pulses by plasma waves, *Phys. Rev. A* **42**, 3526 (1990).
- [21] V. A. Mironov, A. M. Sergeev, E. V. Vanin, G. Brodin, and J. Lundberg, Upper limits for frequency up-conversion in the nonlinear photon accelerator, *Phys. Rev. A* **46**, R6178 (1992).
- [22] S. V. Bulanov, V. I. Kirsanov, F. Pegoraro, and A. S. Sakharov, Charged particle and photon acceleration by wake field plasma waves in nonuniform plasmas, *Laser Phys.* **3**, 1078 (1993).
- [23] A. J. Howard, D. Turnbull, A. S. Davies, P. Franke, D. H. Froula, and J. P. Palastro, Photon acceleration in a flying focus, *Phys. Rev. Lett.* **123**, 124801 (2019).
- [24] J. P. Palastro, J. L. Shaw, P. Franke, D. Ramsey, T. T. Simpson, and D. H. Froula, Dephasingless laser wakefield acceleration, *Phys. Rev. Lett.* **124**, 134802 (2020).
- [25] A. Debus, R. Pausch, A. Huebl, K. Steiniger, R. Widera, T. E. Cowan, U. Schramm, and M. Bussmann, Circumventing the dephasing and depletion limits of laser-wakefield acceleration, *Phys. Rev. X* **9**, 031044 (2019).
- [26] C. Caizergues, S. Smartsev, V. Malka, and C. Thaury, Phase-locked laser-wakefield electron acceleration, *Nat. Photon.* **14**, 475 (2020).
- [27] S. V. Bulanov, V. A. Vshivkov, G. I. Dudnikova, N. M. Naumova, F. Pegoraro, and I. V. Pogorelsky, Laser acceleration of charged particles in inhomogeneous plasmas. I, *Plasma Phys. Rep.* **23**, 259 (1997).
- [28] P. Sprangle, B. Hafizi, J. R. Peñano, R. F. Hubbard, A. Ting, C. I. Moore, D. F. Gordon, A. Zigler, D. Kaganovich, and T. M. Antonsen, Jr., Wakefield generation and GeV acceleration in tapered plasma channels, *Phys. Rev. E* **63**, 056405 (2001).
- [29] E. Guillaume, A. Döpp, C. Thaury, K. Ta Phuoc, A. Lifschitz, G. Grittani, J.-P. Goddet, A. Tafzi, S. W. Chou, L. Veisz, and V. Malka, Electron rephasing in a laser-wakefield accelerator, *Phys. Rev. Lett.* **115**, 155002 (2015).
- [30] S. V. Bulanov, T. Z. Esirkepov, Y. Hayashi, H. Kiriyama, J. K. Koga, H. Kotaki, M. Mori, and M. Kando, On some theoretical problems of laser wake-field accelerators, *J. Plasma Phys.* **82**, 905820308 (2016).
- [31] R. T. Sandberg and A. G. R. Thomas, Photon acceleration from optical to XUV, *Phys. Rev. Lett.* **130**, 085001 (2023).
- [32] J. B. Rosenzweig, Nonlinear plasma dynamics in the plasma wake-field accelerator, *Phys. Rev. Lett.* **58**, 555 (1987).
- [33] See Supplemental Material at <http://link.aps.org/supplemental/10.1103/PhysRevE.109.025210> for the Python functions used to generate the dephasingless profiles.
- [34] S. Weinberg, Eikonal method in magnetohydrodynamics, *Phys. Rev.* **126**, 1899 (1962).
- [35] D. Guénot, D. Gustas, A. Vernier, B. Beaupaire, F. Böhle, M. Bocoum, M. Lozano, A. Jullien, R. Lopez-Martens, A. Lifschitz, and J. Faure, Relativistic electron beams driven by kHz single-cycle light pulses, *Nat. Photon.* **11**, 293 (2017).
- [36] J. Kim, V. L. J. Phung, K. Roh, M. Kim, K. Kang, and H. Suk, Development of a density-tapered capillary gas cell for laser wakefield acceleration, *Rev. Sci. Instrum.* **92**, 023511 (2021).
- [37] A. Akhiezer and R. Polovin, Theory of wave motion of an electron plasma, *J. Exp. Theor. Phys.* **3**, 696 (1956).
- [38] E. Infeld and G. Rowlands, Relativistic bursts, *Phys. Rev. Lett.* **62**, 1122 (1989).
- [39] P. Singh Verma, S. Sengupta, and P. Kaw, Bernstein-Greene-Kruskal waves in relativistic cold plasma, *Phys. Plasmas* **19**, 032110 (2012).
- [40] P. S. Verma, S. Sengupta, and P. Kaw, Breaking of longitudinal Akhiezer-Polovin waves, *Phys. Rev. Lett.* **108**, 125005 (2012).
- [41] P. F. Byrd and M. D. Friedman, *Handbook of Elliptic Integrals for Engineers and Scientists* (Springer, Berlin, 1971).
- [42] T. P. Coffey, Breaking of large amplitude plasma oscillations, *Phys. Fluids* **14**, 1402 (1971).
- [43] J. B. Rosenzweig, B. Breizman, T. Katsouleas, and J. J. Su, Acceleration and focusing of electrons in two-dimensional nonlinear plasma wake fields, *Phys. Rev. A* **44**, R6189 (1991).
- [44] A. Pukhov and J. Meyer-ter Vehn, Laser wake field acceleration: the highly non-linear broken-wave regime, *Appl. Phys. B* **74**, 355 (2002).
- [45] W. Lu, C. Huang, M. Zhou, W. B. Mori, and T. Katsouleas, Non-linear theory for relativistic plasma wakefields in the blowout regime, *Phys. Rev. Lett.* **96**, 165002 (2006).
- [46] W. Lu, C. Huang, M. Zhou, W. B. Mori, and T. Katsouleas, A nonlinear theory for multidimensional relativistic plasma wave wakefields, *Phys. Plasmas* **13**, 056709 (2006).
- [47] A. Golovanov, I. Y. Kostyukov, A. Pukhov, and V. Malka, Energy-conserving theory of the blowout regime of plasma wakefield, *Phys. Rev. Lett.* **130**, 105001 (2023).
- [48] A. Sainte-Marie, O. Gobert, and F. Quéré, Controlling the velocity of ultrashort light pulses in vacuum through spatio-temporal couplings, *Optica* **4**, 1298 (2017).
- [49] D. H. Froula, D. Turnbull, A. S. Davies, T. J. Kessler, D. Haberberger, J. P. Palastro, S. W. Bahk, I. A. Begishev, R. Boni, S. Bucht, J. Katz, and J. L. Shaw, Spatiotemporal control of laser intensity, *Nat. Photon.* **12**, 262 (2018).